



Detection and attribution of upper-tropospheric warming over the tropical western Pacific

Yana Li¹ · Song Yang^{1,2,3} · Yi Deng⁴ · Xiaoming Hu^{1,2} · Ming Cai⁵ · Wen Zhou⁶

Received: 3 September 2018 / Accepted: 11 February 2019 / Published online: 18 February 2019
© The Author(s) 2019

Abstract

Both model and satellite observations suggest that the warming in the tropical upper troposphere is more pronounced than in the lower troposphere. This study describes the tropical upper-tropospheric-warming (UTW) in the ECMWF Reanalysis Interim dataset, and reveals radiative and non-radiative processes contributing to the long-term change in UTW. The maximum intensity of the UTW is found between 250 and 400 hPa with a warming rate about 3K/decade over the tropical Atlantic and western Pacific oceans. The warming is more prominent from boreal winter to early spring than the rest of the year. In the tropical western Pacific, where the warmest ocean water resides, the long-term change in the annual mean UTW is mainly contributed by the variations of atmospheric deep convection and the oceanic dynamical process and heat storage (Ocn) with the latter playing a more important role. The UTW caused by the deep convection is mainly through the latent heat release associated with enhanced upward motion and condensation. The UTW related to Ocn is mainly a result of enhanced upward long-wave radiation from the ocean surface due to the large heat storage in the thermocline. The variations in Ocn mainly contribute to the UTW from winter to early spring, while the changes in deep convection play a more essential role from summer to fall. Also shown by the differences in deep convection, a strengthening of the Walker circulation since the early 2000s is also found in the reanalysis, which is most apparent in boreal summer and fall over the tropical Pacific, facilitating the deep convection to dominate.

Keywords The upper-tropospheric warming · The tropical western Pacific · Long-term change · Attribution analyses

1 Introduction

In the context of global warming, a robust feature in the tropics is the larger upper-tropospheric warming (UTW) than the lower-tropospheric and surface warming, which was predicted by Hansen et al. (2002) and the IPCC (Intergovernmental Panel on Climate Change) TAR (Third Assessment Report) general circulation models (GCMs). The IPCC AR4 (Fourth Assessment Report) more explicitly predicted that such UTW reached its maximum at about 200 hPa and decreased to zero near the tropical tropopause, although the feature might have been overestimated (Song et al. 2014). Moreover, the IPCC AR5 (Fifth Assessment Report) also reviewed this tropical UTW in Chap. 12 by Collins et al. (2013), showing a similar pattern to the former prediction with various magnitudes under different scenarios. Aside from the IPCC GCM simulation, previous studies also conducted observational verifications. For example, Fu and Johanson (2005) applied satellite-borne Microwave Sounding Unit observations of 1987–2003 to demonstrate that the

✉ Song Yang
yangsong3@mail.sysu.edu.cn

¹ School of Atmospheric Sciences, Sun Yat-sen University, 135 West Xingang Road, Guangzhou 510275, China

² Guangdong Province Key Laboratory for Climate Change and Natural Disaster Studies, Sun Yat-sen University, Guangzhou, China

³ Southern Laboratory of Ocean Science and Engineering, Sun Yat-sen University, Zhuhai, China

⁴ School of Earth and Atmospheric Sciences, Georgia Institute of Technology, Atlanta, GA, USA

⁵ Department of Earth, Ocean, and Atmosphere Science, Florida State University, Tallahassee, FL, USA

⁶ School of Energy and Environment, City University of Hong Kong, Hong Kong, China

tropical troposphere warmed faster than the surface and that the trends of tropical tropospheric temperature increased with height, which confirms the GCM prediction from IPCC TAR. Fu et al. (2011) further proved the prediction from IPCC AR4 and by analyzing the same data set as in Fu and Johanson (2005) from 1987 to 2010.

The tropical UTW is associated with the climate sensitivity due to its impact on climate feedback processes as water vapor, lapse rate, cloud feedback, and atmospheric dynamics (Colman 2001; Hartmann and Larson 2002; Bony et al. 2006). A tropospheric warming that is larger at the upper levels than at the low levels has a directly negative effect on the lapse rate, which reduces the lapse rate leading to a negative radiative feedback and further affects the water vapor feedback (Bony et al. 2006; Soden and Held 2006). Spatial and temporal variations of the globally zonal mean UTW have been extensively studied using observational evidences and numerical experiment results, such as in Thorne et al. (2007); Santer et al. (2008); Christy et al. (2007, 2010), and others. While the UTW has been gradually proved in observations and predicted by models, large inter-model spreads of uncertainty still exist, due mainly to the currently poor understanding of climate feedback processes (Colman 2001; Fu and Johanson 2005). Before discussing the impact of such UTW on climate feedback processes, the reverse impact (i.e., the formation of the UTW via the impact of climate feedback on it) deserves detailed analyses. Song et al. (2014) applied a coupled atmosphere-surface “climate feedback-response analysis method” (CFRAM) to quantify the contributions of climate feedbacks to global tropospheric warming in the NCAR CCSM3.0 (Community Climate System Model Version 3.0 of National Center for Atmospheric Research) model due to a doubling of CO₂ concentration, and concluded that convective process and water vapor feedback are the two major contributors to the tropical upper-tropospheric temperature change. In this study, we will apply this CFRAM developed by Lu and Cai (2009) and Cai and Lu (2009) to elucidate the formation of the tropical UTW by quantifying the relative contributions of each feedback process based on reanalysis data. The methodology will be detailed in Sect. 2.

As Ramage (1968) demonstrated, the tropical land generates a much greater amount of heat for export than the equatorial oceanic regions and the troposphere over the Maritime Continent in boreal winter is probably the single greatest energy source for the extratropical atmospheric circulation. Thus, as a secular tropical heating source, the latent heat released from the deep convection over the tropical western Pacific dominates that over other tropical regions and plays an important role in modulating global climate. Located amid the monsoon system, the deep convection over this region strongly interacts with the monsoon circulation. For example, the latent heat released by the enhanced convection

in this region caused by strengthened northerly winds along the east coastline during strong East Asian winter monsoon events in turn strengthens the winter monsoon by enhancing the upper branch of local meridional circulation and accelerating the upper-tropospheric East Asian westerly jet stream (Yang and Webster 1990; Yang et al. 2002; Chang et al. 2004). The energy generated from the released latent heat can also exert an impact on the climate over not only East Asia, but also North America and Europe via teleconnection patterns such as the Pacific-Japan pattern and Pacific-North American pattern (He and Wu 2014; Ding et al. 2011). The anomalous circulation of the Pacific-Japan pattern, in turn, can intensify the regional convective activity via enhancing evaporation and moisture convergence and dynamically inducing anomalous ascent (Kosaka and Nakamura 2010; Wu et al. 2014). As Gill (1980) illustrated a considerable east-west asymmetric circulation by solutions for heating concentrated in a region of finite extent, the intensity and center of tropical heating also indicate the zonal tropical circulation such as that related to the El Niño-Southern Oscillation. Thus, the variation of the tropical heating over the tropical western Pacific (i.e., the UTW) can exert major impacts on global climate variations. Thus, this study will be mainly focused on the formation of the UTW over the tropical western Pacific.

The major objectives of the present work are: (1) to describe the observed long-term change in the UTW over the tropical western Pacific; (2) to address which radiative or non-radiative process is the main contributor to the formation of the long-term change; and (3) to understand how the variation of the main processes contributes to the long-term change in UTW.

Data and methods will be described in Sect. 2. Section 3 discusses the spatial and temporal variations of UTW. Attribution analyses of long-term change in UTW based on annual and monthly mean data will be presented in Sects. 4 and 5, respectively. Section 6 summarizes the major findings of this study.

2 Data and methods

The primary data set used in this study is the European Centre for Medium-range Weather Forecasts Reanalysis Interim (ERA-Interim, Dee et al. 2011). It covers the period from 1979 to the present and has a horizontal resolution of 1° longitude × 1° latitude with 37 pressure levels in the vertical ranging from 1000 to 1 hPa. Monthly outgoing long-wave radiation (OLR) from National Oceanic and Atmospheric Administration with a horizontal resolution of 2.5° by 2.5° is also used in this study.

The major analysis tool is the CFRAM, same as the method applied in Song et al. (2014), which is based on

the total energy balance within an atmosphere-surface column. We consider the total energy balance equation (Deng et al. 2012; Yang and Ren 2017) separately for one decade as 1985–1996 and the other decade as 2004–2013, take the difference (Δ) between the two decades (i.e., 2004–2013 minus 1985–1996), and then obtain

$$\Delta \frac{\partial E}{\partial t} = \Delta S - \Delta R + \Delta Q^{non-radiative}, \tag{1}$$

where S (R) is the vertical profile of the net convergence (divergence) of short-wave (long-wave) radiation flux within each layer. Above the surface, $\Delta Q^{non-radiative}$ is the vertical profile of the convergence of total energy due to atmospheric turbulent, convective, and advective motions. At the surface, $\Delta Q^{non-radiative}$ corresponds to the loss of energy due to surface heat fluxes, as well as the net energy convergence in the ocean mixed layer if the surface is over ocean. The elements of $\frac{\partial E}{\partial t}$ represent change in the rate of energy storage. All terms in Eq. (1) are in units of W/m^2 .

As in Li et al. (2017), we express ΔS and ΔR as the sum of partial radiative energy flux convergence/divergence perturbations due to individual radiative feedback processes:

$$\Delta S \approx \Delta S^{solar} + \Delta S^{wv} + \Delta S^{cloud} + \Delta S^\alpha + \Delta S^{CO_2} + \Delta S^{O_3} \text{ and } \Delta R \approx \Delta R^{wv} + \Delta R^{cloud} + \Delta R^{CO_2} + \Delta R^{O_3} + \Delta T \frac{\partial R}{\partial T} \tag{2}$$

In Eq. (2), superscripts “solar”, “wv”, and “ α ” represent solar insolation, water vapor, and surface albedo, respectively. $\frac{\partial R}{\partial T}$ is the Planck feedback matrix. Substituting Eq. (2) into Eq. (1), rearranging the terms, we obtain

$$\Delta T = \left(\frac{\partial R}{\partial T}\right)^{-1} \left\{ \Delta S^{solar} + \Delta(S - R)^{wv} + \Delta(S - R)^{cloud} + \Delta(S - R)^{CO_2} + \Delta(S - R)^{O_3} + \Delta S^\alpha + \Delta Q^{ATD} + \Delta Q^{surf} \right\} \tag{3}$$

The variables required as input to the radiative transfer model (Fu and Liou 1992, 1993) including solar insolation at the top of the atmosphere (TOA), air/surface temperatures, specific humidity, cloud amount, cloud liquid/ice water content, surface albedo, and ozone mixing ratio are all obtained from the ERA-Interim. ΔQ^{ATD} in Eq. (3) is zero at the surface layer, and $\Delta Q^{ATD} = -\Delta(S - R)_{atmos}$ in the atmospheric layers, representing the vertical profile of the energy perturbation in the atmosphere associated with atmospheric motions (including turbulent, convective (i.e., the latent heat release and adiabatic warming/cooling), and large-scale motions) and heat storage anomalies (expected to be very small), which is named as atmospheric dynamical process (ATD). ΔQ^{surf} is zero in atmosphere layers and $\Delta Q^{surf} = -\Delta(S - R)_{surf}$ at the surface layer, representing the energy perturbation at the surface due to surface turbulent sensible (ΔQ^{sshf}) and latent (ΔQ^{slhf}) heat flux anomalies, the changes in the rate of heat storage (of land or oceans) and the oceanic circulation if the surface is over oceans. The sum

of the oceanic dynamics and land/ocean heat storage term (Ocn) is estimated as the residual of the surface energy balance equation, $\Delta Q^{Ocn} = -\Delta(S - R)_{surf} - (\Delta Q^{sshf} + \Delta Q^{slhf})$. Equation (3) allows us to express the vertical profile of the temperature difference between two specific decades or months in the atmosphere-surface column at a given horizontal grid as the sum of the vertical profiles of the partial temperature changes (PTCs) due to the changes in solar insolation, water vapor, cloud, surface albedo, atmospheric dynamics, and oceanic dynamics and ocean/land heat storage.

To quantify the relative contributions of each individual process to 3D temperature anomalies between 250 and 400 hPa over a certain region based on its spatial pattern and mean amplitude, we compute the pattern-amplitude projection (PAP_i) using the partial temperature anomalies (ΔT_{iz}) in layer Z associated with each individual process i . Following Park et al. (2012), we have

$$PAP_i = \frac{\frac{1}{Z \times A} \int_Z \int_A a^2 \Delta T \Delta T_i \cos \phi d\lambda d\phi}{\frac{1}{Z \times A} \int_Z \int_A a^2 (\Delta T)^2 \cos \phi d\lambda d\phi} \tag{4}$$

where ϕ and λ are latitude and longitude, respectively, a is the mean radius of the earth, ΔT is the observed temperature anomalies, Z is the vertical level, and A represents the region over which spatially averaged values are computed.

By definition, the sum of PAP coefficients at a certain layer is one (K). The difference between an area-averaged PTC and a PAP is that the latter emphasizes the “spatial similarity” between the PTC distribution and the total temperature change distribution and is thus a better metric for assessing the overall contribution of a specific process to the temperature change over the region considered.

3 Characteristics of UTW

The pattern of tropospheric warming (TW) trends at 250–1000 hPa (Fig. 1a) indicates that the warming over the middle- and high-latitudes is stronger than that over the lower latitudes, and the Northern Hemisphere warms faster than the Southern Hemisphere. In the tropics, significant warming covers the tropical Atlantic, the tropical Indian Ocean, and the tropical western Pacific. The IPCC AR4 has demonstrated that in the context of global warming,

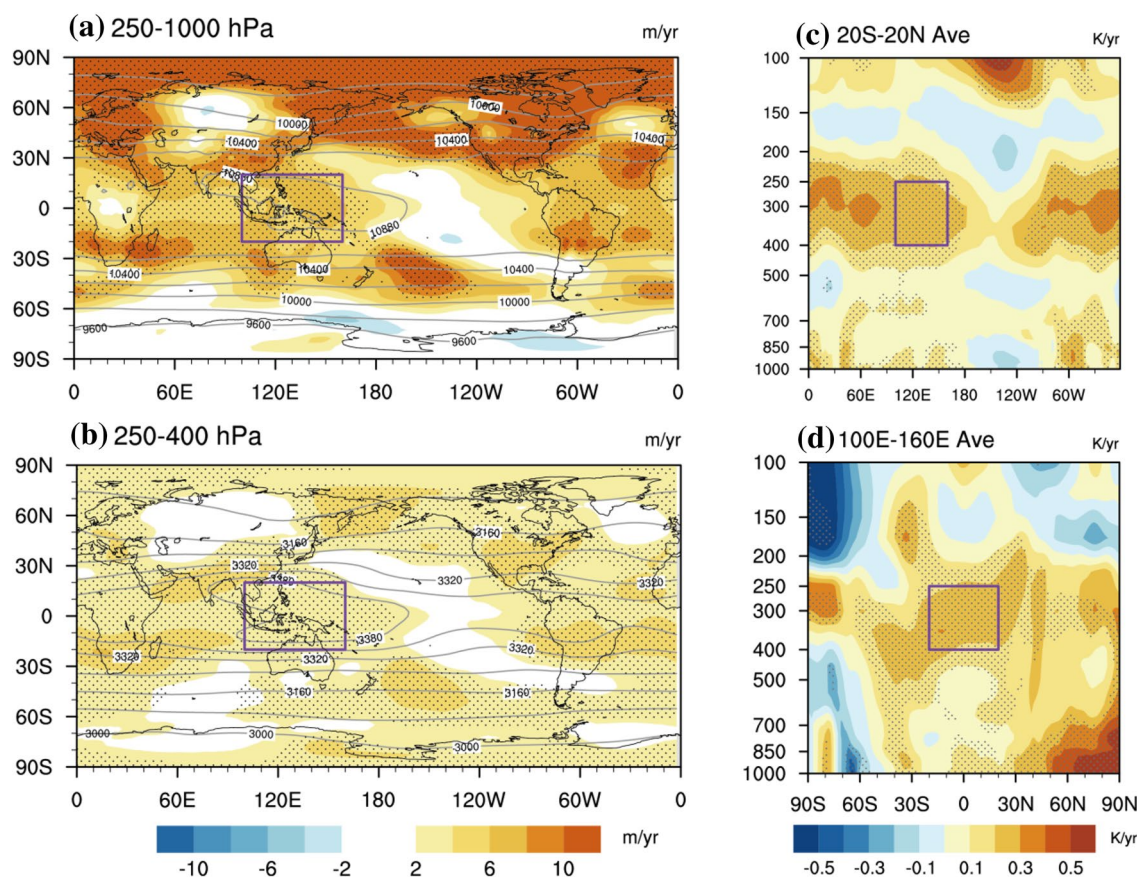


Fig. 1 Trends (shading; m/yr) of **a** 250–1000-hPa and **b** 250–400-hPa air thickness in 1979–2015, with the respective climatology in 1981–2010 (contours; m). Vertical distributions of areal average of tem-

perature trends over **c** 20°S–20°N and **d** 100°–160°E. Stippled areas indicate values significant at the 99% confidence level. Purple boxes in each panel indicate the analysis area

the upper troposphere especially above 400 hPa warms faster than the surface. The TW trends at 250–400 hPa are shown in Fig. 1b, which presents that the spatial distribution over the tropics resembles that in Fig. 1a, while the UTW over the high latitudes is not as strong as the warming at 250–1000 hPa, indicating that the lower-tropospheric and surface warming mainly contributes to the total TW over the high latitudes. Over the eastern Indian Ocean, the Maritime Continent, and the tropical western Pacific, the troposphere is the warmest area in the tropics (see contours), which also reveals a relatively high warming rate. Thus, we will focus on these regions from 100 to 160°E as shown by the purple box (Fig. 1a, b) in the following analysis. The vertical distribution of TW weighted averaged over 20°S–20°N depicts a pronounced UTW between 200 and 500 hPa with a higher magnitude (> 2 K/decade) in 250–400 hPa over the whole tropical region except the eastern tropical Pacific (Fig. 1c). Compared with the magnitude and amplitude of the UTW, the surface warming is relatively weaker globally and even presents cooling trends in the eastern tropical Pacific. The meridional-vertical distribution of TW

averaged over 100°–160°E shows a significant warming core over 30°S–30°N between 200 and 500 hPa, with the strongest over 250–400 hPa (Fig. 1d). Another pronounced warming area is located in the lower troposphere north of 60°N, mainly concentrated below 700 hPa, also known as the Arctic warming (e.g., Cai 2005; Graversen et al. 2008).

UTW over 20°S–20°N/100°–160°E shows an interdecadally strengthening trend with a stronger interannual variation before the late-1990s, exactly in 1998, and a weaker interannual variation since then (Fig. 2). This feature is depicted more clearly by the 5-yr smoothing result as shown by the solid black curve in Fig. 2. The warming trend of UTW seems more prominent since the late-1990s, although the global surface warming experienced a hiatus of debate (Guan et al. 2015; Hu et al. 2017). We use two periods, 1986–1995 and 2004–2013, to represent the anomalously cooling and warming decades to demonstrate the main contributors to the interdecadal warming (IDW) by analyzing the changes in the radiative and non-radiative (dynamic and thermodynamic) processes between these two periods.

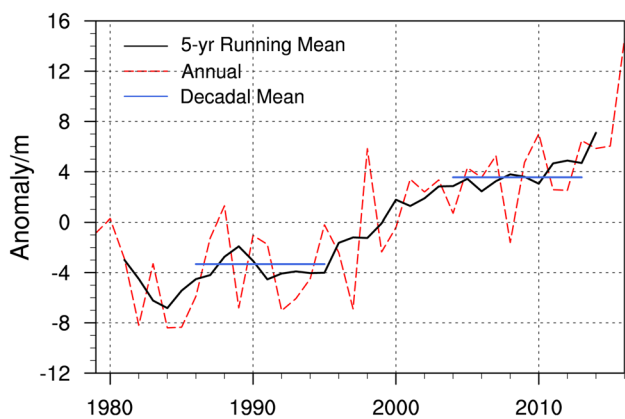


Fig. 2 Annual mean of 250–400-hPa air thickness anomalies over 20°S–20°N/ 100°–160°E (red dashed curve; m) based on the climatology of 1981–2010. The solid black line shows the 5-yr running mean values (m). The blue lines show the mean values of 1986–1995 and 2004–2013

4 Long-term change in UTW based on annual mean data

4.1 Attribution analysis

Based on the CFRAM analysis, the contributions of individual processes to the change in the mean temperature over 250–400 hPa between 1986 and 1995 and 2004–2013 are quantitatively revealed by their PTCs. As the spatial patterns shown in Fig. 3, the change in each variable of solar insolation, surface albedo, ozone, CO₂, and water vapor contribute to the IDW at a magnitude about 0.1 K. Specifically, the changes in solar insolation contribute positively (positive PTCs) south of 10°S and negatively (negative PTCs) north of 10°N, due mainly to its interdecadal variation. The variation of surface albedo provides a positive contribution to the IDW over the Maritime Continent and the tropical western Pacific. PTCs caused by changes in ozone are uniformly negative while that caused by the change in CO₂ is uniformly positive with a large contribution band between 10°S and 10°N. Also, the more (less) water vapor over land and the

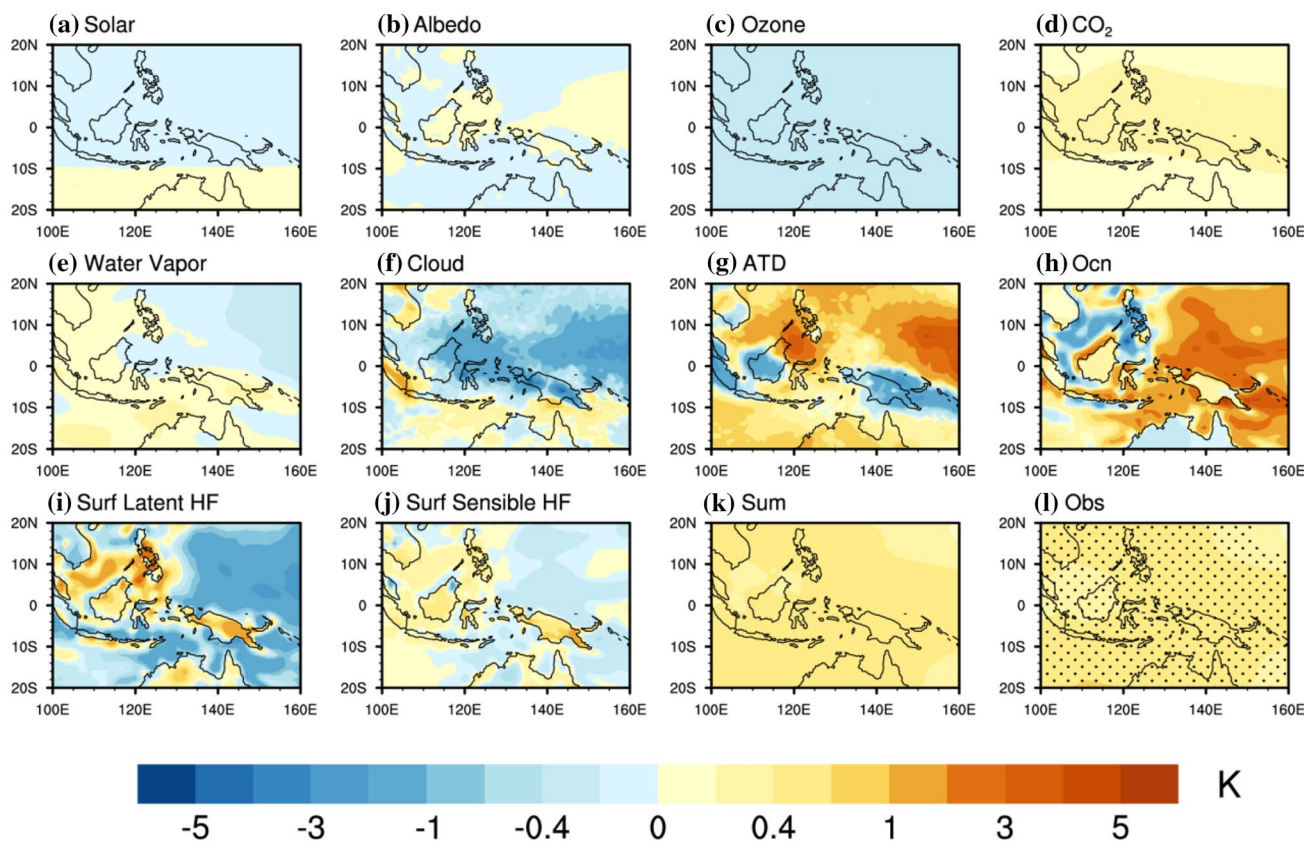


Fig. 3 Weighted mean PTC at 250–400 hPa due to changes in **a** solar insolation at the top of the troposphere, **b** surface albedo, **c** ozone, **d** CO₂, **e** water vapor, **f** cloud, **g** atmospheric dynamic processes, **h** oceanic dynamical process and heat storage, **i** surface latent heat flux,

j surface sensible heat flux. And **k** is the sum of the PTCs of (a–j). Observations are shown in (l) with values significant at the 95% confidence level dotted

eastern Indian Ocean (the western Pacific) contributes to the UTW positively (negatively). Moreover, the change in cloud as a radiative process contributes negatively north of 5°S due to more cloud and slightly positively south of 10°N resulting from less cloud. Overall, among all the radiative processes, cloud exerts the largest impact on the IDW.

The change in ATD warms most of the analysis region especially over the ocean domain north of 0°N, except the cooling effect over land. By the function of upward long-wave radiation from the surface, the change in Ocn warms the region, with the largest contribution over the ocean east of 120°E, aside from the cooling effect over the southern South China Sea (SCS) and northern Australia. The spatial pattern of PTCs due to the change in surface latent heat flux (SLHF) resembles the opposite feature that is due to Ocn but with an opposite sign. The PTCs induced by the change in surface sensible heat flux (SSHF) exhibit a pattern similar to those caused by SLHF but with a smaller magnitude. Figure 1k shows the total temperature change calculated by adding all the PTCs of each individual process, which resembles the observed feature shown in Fig. 1l.

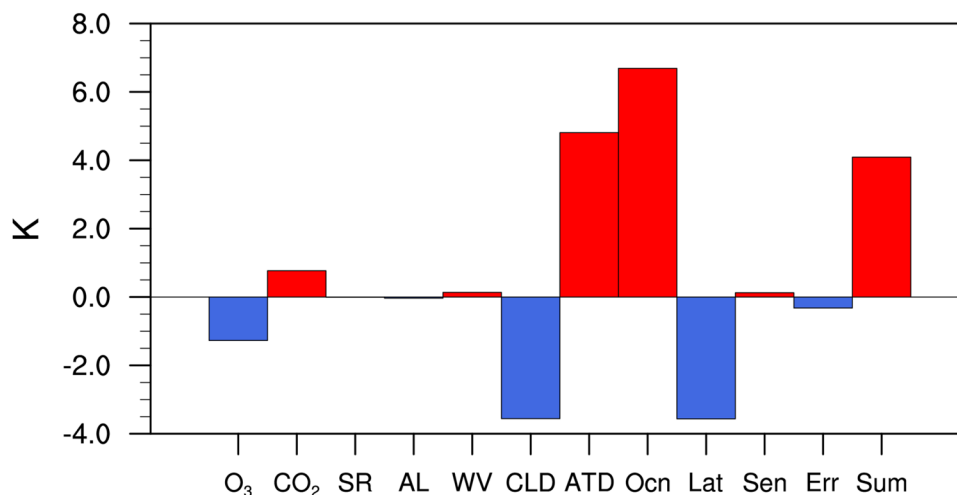
Based on the spatial distribution of the PTCs of each process, we explicitly illustrate the relatively essential contributions by the variations of cloud, ATD, Ocn, and SLHF to the formation of UTW by analyzing their PAP coefficients, which quantify the relative contributions of each process from both the spatial pattern and magnitude. An analysis of PAP indicates that the changes in ATD and Ocn are the two largest positive contributors to the UTW over 20°S–20°N/100°–160°E, with CO₂ as a secondary contributor, while variations of cloud and SLHF are the two largest negative contributors, with ozone as a third one (Fig. 4). The negative contribution of variations of cloud is mainly related to the increase in the middle and high clouds (figure not shown). And the offline error is negligible. Thus, the long-term change in the annual mean UTW over the tropical

western Pacific is mainly modulated positively by ATD and Ocn and negatively by cloud and SLHF.

4.2 Long-term change in oceanic processes

As discussed before, the UTW caused by the change in Ocn occurs mainly via upward long-wave radiation from the surface, which is associated with the oceanic thermal status and dynamical process (here, land heat content is negligible). The forcing due to the variation of Ocn (Fig. 5a) shares the same spatial distributions as the PTCs (Fig. 3h). Here, a positive value means that energy is transferred from oceans to the atmosphere, and vice versa. Compared with the long-term change in the heat content of the 0–200-m mixed layer, the enhanced forcing over the ocean surface east of the Maritime Continent is contributed mainly by the more heat storage in the mixed layer, which is a result of the enhanced easterly trade wind. The long-term change in the heat content in the mixed layer shows a strengthened zonal gradient, with a thicker thermocline in the tropical western Pacific and a thinner thermocline in the tropical eastern Pacific (figure not shown), and the impact of such an enhanced gradient on the atmospheric circulation will be discussed in the following sub-section. The change in the oceanic dynamics plays a key role in the southern SCS, working against the warming effect of enhanced heat content in the mixed layer, leading to a net cooling effect on the surface temperature. As shown by the contours in Fig. 5a, the long-term change in surface heat fluxes including SLHF and SSHF are well collocated with the distribution of forcing, as the anomalous downward transport over the negative forcing and the enhanced upward transport over the positive forcing, which is also induced by the enhanced surface trade wind. Moreover, the long-term change in Ocn exerts an impact on the atmospheric circulation via anomalous heat fluxes. Thus, the overall positive

Fig. 4 Pattern-amplitude projection coefficients (PAPs) of attributions of each term to the annual mean temperature differences between 1986 and 1995 and 2004–2013 over 250–400 hPa/20°S–20°N/100°–160°E. Labels from left to right refer to ozone, CO₂, surface albedo, water vapor, cloud, ATD, Ocn, SLHF, SSHF, the offline error, and the sum of all the above processes, respectively



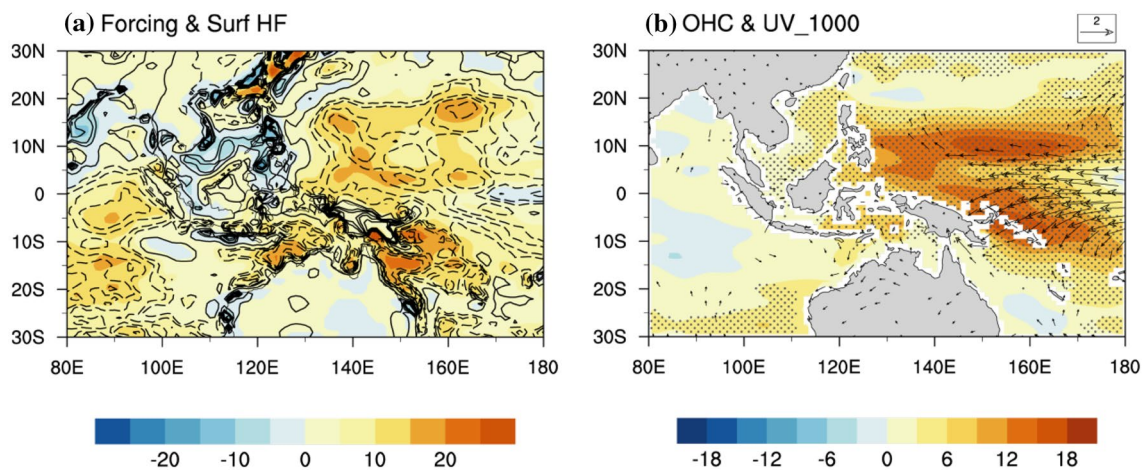


Fig. 5 **a** Differential forcing (shading; W/m^2) and surface heat fluxes [contours; $J/(m^2*s)$], and **b** differential ocean heat content in the 0–200-m mixed layer (shading; $1e5 J/m^2$) and 1000-hPa wind

between 1986 and 1995 and 2004–2013. Vectors and dotted areas indicate values significant at the 95% confidence level

contribution by Ocn results from the enhanced ocean heat content in the mixed layer over the tropical western Pacific.

4.3 Long-term changes in atmospheric processes

Both the horizontal and vertical temperature transport strengthens over the research domain (figure not shown), and the latter is one order larger than the former. Following

analyses are mainly focused on the long-term change in the vertical motion. Accompanied by the enhanced deep convection (indicated by OLR shown as the red curve in the lower panel of Fig. 6), significantly stronger ascending motion occurs mainly over $20^{\circ}S-5^{\circ}N/110^{\circ}-160^{\circ}E$. An enhanced zonal circulation is observed in the tropics, with the more-eastward upward branch located over the ocean northeast of Australia. As shown in Fig. 6a, anomalous upward motion

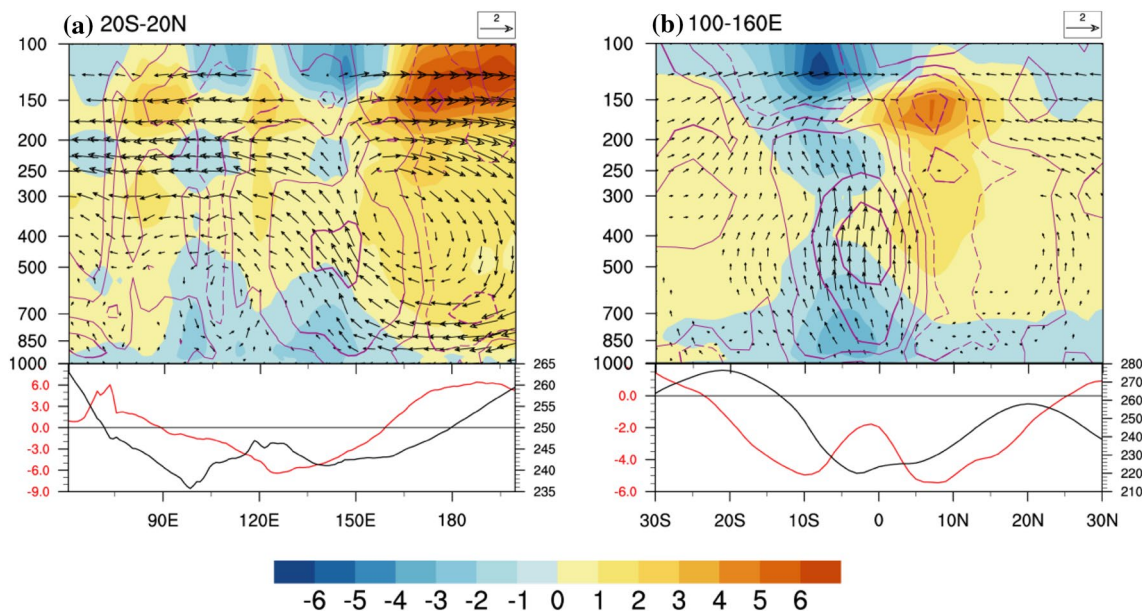


Fig. 6 Vertical distribution of **a** $20^{\circ}S-20^{\circ}N$ meridional mean and **b** $100^{\circ}-160^{\circ}E$ zonal mean PTCs due to changes in ATD (shading; K), diabatic heating rate anomalies (purple contours; K/day), and vertical motion anomalies (vectors; m/s) between 1986 and 1995 and 2004–

2013. Thicker lines and vectors indicate values significant at the 90% confidence level. Curves at the bottom are the corresponding anomalous OLR (red) and OLR climatology (black) for 1981–2010

is mainly located between 130 and 160°E, while the anomalously strengthened deep convection presents between 90 and 150°E. The long-term change in diabatic heating from the latent heat release of condensation exerts a warming effect between 110 and 160°E with a center around 150°E. The UTW in 250–400 hPa caused by ATD is mainly contributed by diabatic heating, which works against the adiabatic cooling of enhanced upward motion. The strengthened upward branch of the Hadley Cell is located over 20°S–5°N and centered between 10 and 0°N (Fig. 6b), while enhanced rainfall occurs between 20 and 20°N. Although diabatic heating is also enhanced, the total effect of ATD is to cool the troposphere over 10°S–0°N, implying that adiabatic cooling plays a key role. However, accompanied by such

enhanced deep convection over the southern part, anomalous downward motions dominate over the northern portion of the domain (between 0° and 20°N) with less diabatic warming released. Thus, the UTW at 250–400 hPa over 0°–20°N is a result of enhanced adiabatic warming and weaker diabatic cooling. As the warming in the north is more dominant than the cooling in the south, overall warming exists at 250–400 hPa for the whole region. Therefore, the UTW induced by the ATD at 250–400 hPa in the region of consideration is mainly contributed by the interdecadally enhanced deep convection over 20°S–5°N/110°–160°E.

5 Long-term changes in UTW based on monthly mean data

5.1 Attribution analysis

A further analysis of the long-term variations based on monthly mean data is expected to reveal more detailed characteristics of the UTW. The vertically-weighted mean temperature over 250–400 hPa/20°S–20°N/100°–160°E between the 2 decades is in the range of about 0.24–0.75 K. As illustrated in Fig. 7, the UTW peaks from December to March and is relatively weak in boreal summer and fall except in July and September.

Figure 8 depicts the PAP results for long-term variation based on the CFRAM analysis using monthly data, similar to the results shown in Fig. 4 using annual mean data. As relatively weaker contributors, ozone and CO₂ act as consistently negative and positive contributors all year round. Relatively larger contributors in each month are the same as those for the annual mean, which include Ocn, ATD, SLHF,

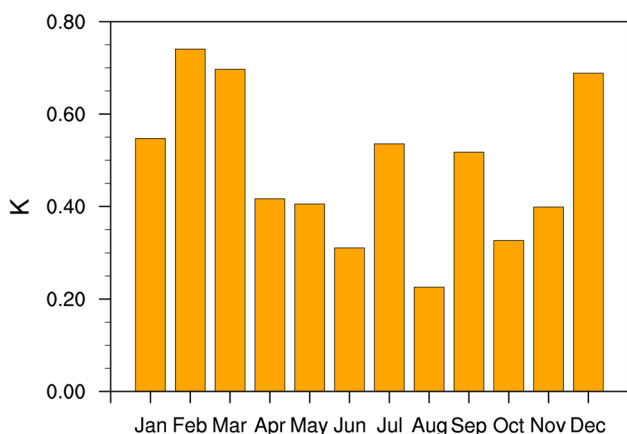
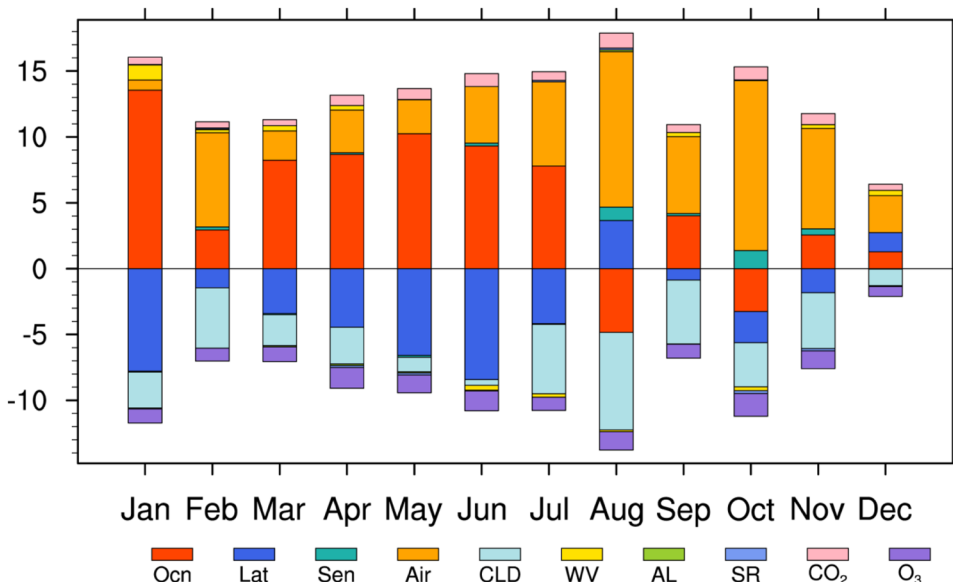


Fig. 7 Differences in vertically weighted mean of monthly temperature between 1986 and 1995 and 2004–2013 over 250–400 hPa/20°S–20°N/100°–160°E

Fig. 8 Same as Fig. 4, but for PAPs in each month



and cloud. The two main negative contributors for the annual mean, SLHF and cloud, show various seasonal variations: SLHF dominates in January-to-June, except February, and cloud plays an essential role in July-to-December. The two prominent positive contributors, Ocn and ATD, also exhibit different seasonal variations. Comparison of the PAP coefficients indicates that Ocn plays a key positive role from January to July, while ATD is the main contributor from August to December, which is similar to the seasonal evolution of SLHF and cloud. Thus, the UTW with various magnitudes in each month is modulated by different main radiative and non-radiative processes. Overall, the main positive contributor to the UTW in boreal winter and spring is Ocn, while that to the UTW in boreal summer and fall is ATD. Next we will briefly focus on the long-term changes in Ocn and ATD based on the seasonal mean instead of the monthly mean.

5.2 Long-term changes in oceanic processes

In boreal winter (Fig. 9a), the spatial pattern of Ocn forcing resembles that of the annual mean in Fig. 5a, with a strongly positive forcing center over the tropical western Pacific and anomalous negative forcing over the southern SCS that is

not so pronounced as that shown by the annual mean. In boreal spring (Fig. 9b), almost all areas show positive forcing with a weaker strength than that in winter, while negative anomalies still exist in the southern SCS. In boreal summer (Fig. 9c), negative anomalies expand from the Bay of Bengal to the western Pacific east of the SCS, and also appear from the eastern Indian Ocean to northwestern Australia. Moreover, the positive forcing anomaly center moves eastward over 160°–180°E. Such differences in the seasonal variations of forcing between the southern and northern SCS also indicate differences in properties of the two parts (Lau et al. 2002). In boreal fall, negative forcing anomalies dominate and cover nearly the entire SCS and eastern Indian Ocean while positive anomalies further weaken and move eastward. Thus, as positive forcing gradually weakens and later moves out of the tropical western Pacific and negative forcing gradually strengthens and expands over the SCS, the positive contribution of Ocn fades from winter to fall or even turns into a negative contribution in fall. Moreover, as the anomalous surface heat fluxes indicate, the impact of Ocn on the atmospheric circulation also gradually weakens from winter to fall.

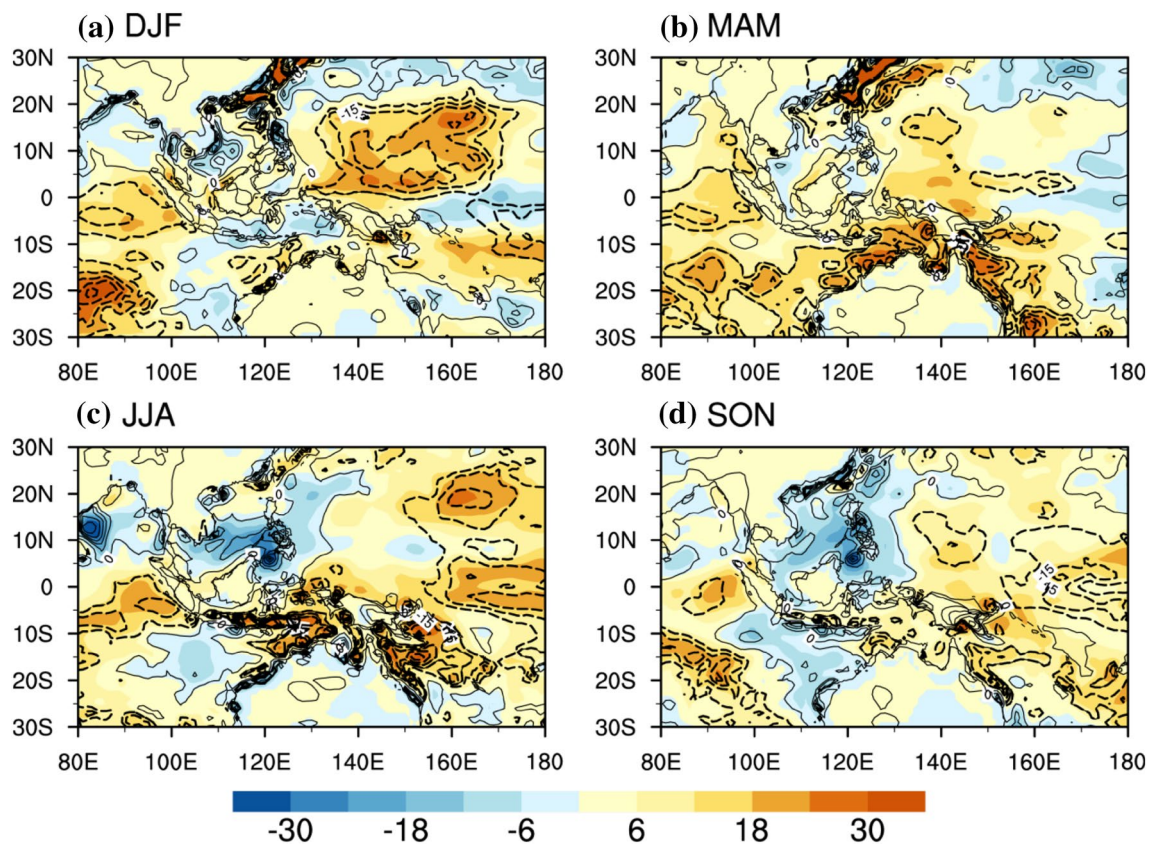


Fig. 9 Same as Fig. 5a, but for each season

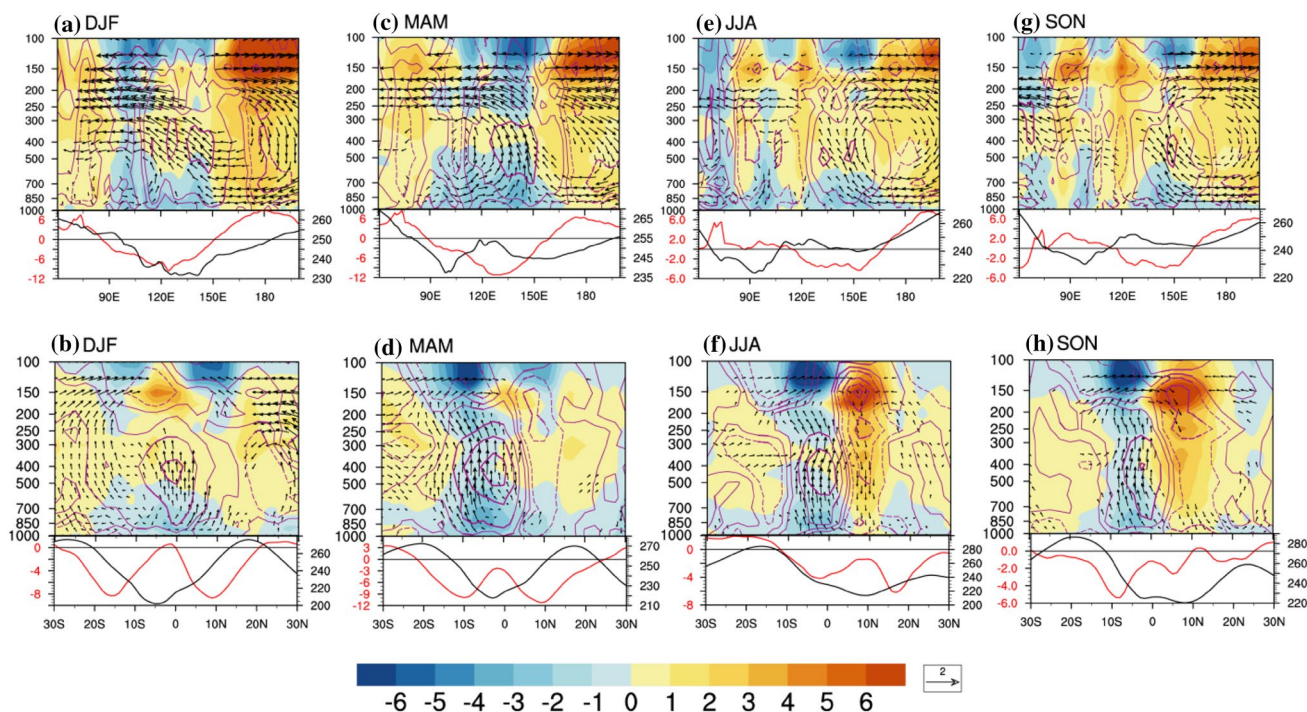


Fig. 10 Same as Fig. 6, but for each season

5.3 Long-term changes in atmospheric processes

The PTC contributed by ATD is modulated by the long-term variations of atmospheric non-radiative processes, which can be elucidated by the variations of temperature advection and adiabatic heating rate. As indicated by the variation of zonal circulation (Fig. 10a, c, e, g), enhanced convection mainly occurs over 130° – 160° E. Specifically, the anomalous upward branch is broadened and tilted westward with height, and easterly anomalies are much enhanced in winter (Fig. 10a) and spring (Fig. 10c), resulting in a strengthened zonal circulation over the Indian Ocean. The upward branch is significantly strengthened over 140° – 160° E without a clear tilt in summer (Fig. 10e) and fall (Fig. 10g), indicating that a pronounced zonal circulation is located over the tropical central and eastern Pacific. With such an interdecadally strengthened upward motion, the adiabatic heating released by condensation also shows an enhanced tendency with the strongest centers over 120° – 150° E in winter and spring and over 130° – 160° E in summer and fall. As shown by the PTC, the increased strength of adiabatic heating is more apparent than that of adiabatic cooling caused by enhanced upward motion, which is even prominent in summer and fall. Accompanied by the seasonally anomalous circulation, deep convection also shows obvious long-term variations (red curves in the upper panels of Fig. 10). In winter, enhanced precipitation is located mainly over 90° – 150° E, and the deep

convection moves slightly westward. From spring to fall, deep convection shows a more eastward location, especially in summer and fall, which should be involved with the aforementioned strengthened zonal circulation over the tropical Pacific.

As the long-term change in meridional circulation shows (Fig. 10b, d, f, and h), enhanced vertical circulation is located mainly over 10° S– 10° N. In winter, upward anomalies are concentrated between 5° S and 5° N, while significantly enhanced precipitation is located around 10° S and 10° N. As the adiabatic cooling is compensated by the diabatic warming that dominates in the region that we focus on, the PTC is positive in the meridional direction. From spring to summer, anomalous upward motion is pronounced south of the equator, and anomalous downward motion is located north of the equator. The negative PTC in the upper troposphere south of the equator is a result of stronger adiabatic cooling (than diabatic warming), which is reversal over north of the equator where the stronger adiabatic warming (than diabatic cooling) leads to positive PTC in the upper troposphere. Such anomalous circulation features are much more prominent in summer and fall. The meridional distribution of deep convection shows a complicated seasonal variation. In boreal winter and spring, significantly enhanced precipitation occurs around 10° S and 10° N, heavier than that near the equator. Enhanced precipitation is located mainly north of the equator in

summer and south of the equator in fall. The aforementioned anomalous downward motion north of the equator weakens the convection in situ, which somehow indicates that the upward branch of meridional circulation is more southward in the later decade. Thus, in all seasons the enhanced vertical circulations over 10°S – 0° / 140° – 160°E exert positive contributions to the UTW. Because of the relatively stronger adiabatic cooling and the enhanced westward advection in the upper troposphere in winter and spring, the positive impact of ATD is weaker than that of Ocn in these seasons. From summer to fall, both diabatic heating and adiabatic warming provide positive contributions so that ATD is the dominant contributor to the UTW in August-to-December and February.

6 Conclusions

The fact that in the tropics the tropospheric temperature trends are larger than the surface warming trends has been studied previously using model outputs and satellite and radiosonde observations. In this study, we revisit this phenomenon using reanalysis data and further illustrate the radiative and non-radiative contributions to the formation of UTW using a climate feedback-response analysis method.

In the tropics, the UTW is pronounced over 250–400 hPa except over the eastern Pacific. Since climatologically the warmest 250–400-hPa UTW is located over the tropical western Pacific, the present study focuses on the UTW over 20°S – 20°N / 100° – 160°E , where a significant interdecadal variation occurred in the air thickness at 250–400 hPa in the late 1990s. Thus, we choose two periods, 1986–1995 and 2004–2013, to represent the anomalously cooling and warming decades, respectively. To analyze the main contributors to this long-term change in the warming, CFRAM analysis is applied to quantify the contributions of radiative and non-radiative (dynamic and thermodynamic) processes.

As revealed by the annual mean data, the changes in Ocn and ATD are the two largest positive contributors while the variations in clouds and SLHF are the two main negative contributors. The cooling effect of ozone and the warming effect of CO_2 are two secondary factors that contribute to UTW. The positive contribution by Ocn is via enhanced upward long-wave radiation due to the large heat storage in the mixed layer. The positive contribution by ATD is modulated mainly by the enhanced diabatic heating induced by the strong convection over the tropical western Pacific, specifically over 10°S – 0° / 140° – 160°E , while the adiabatic warming north of the equator also provides a contribution.

This study further discusses the long-term change for each month. The UTW is strongest in boreal winter from December to March and relatively weaker in summer and fall. The main positive and negative contributors vary with seasons. The prominent feature is that Ocn plays a key role in the formation of UTW in boreal winter and spring while ATD exerts a main impact in boreal summer and fall. Among the negative contributors, SLHF significantly affects the UTW in January-to-June and cloud plays an essential role in July-to-December. The strong and positive contribution of Ocn in winter and spring is modulated by the enhanced ocean heat content in the mixed layer over the tropical western Pacific. This contribution gradually weakens and “leaves” the tropical western Pacific while the negative forcing centered over the SCS gradually strengthens and expands, and as a result the positive contribution of Ocn diminishes from winter to fall and even turns into a negative contribution in fall. ATD exerts positive contributions to the UTW in all seasons. In boreal winter and spring, adiabatic cooling is relatively stronger, and with enhanced westward advection in the upper troposphere the positive impact of ATD is weaker than that of Ocn. In boreal summer and fall, both diabatic heating and adiabatic warming make positive contributions and ATD is the dominant contributor of the UTW. Moreover, a strengthened zonal circulation in the tropics is also observed over both the Indian and the Pacific Oceans, and that over the Pacific is pronounced in summer and fall, facilitating the ATD to dominate.

Acknowledgements The study was supported by the National Key Research and Development Program of China (2016YFA0602703), the National Natural Science Foundation of China (Grants 41690123, 41690120, 91637208, and 41661144019), the “111-Plan” Project of China (Grant B17049), and the Jiangsu Collaborative Innovation Center for Climate Change. Yi Deng is supported by the National Science Foundation under grants AGS-1354402 and AGS-1445956. The ERA-Interim reanalysis used in this study was provided by the European Centre for Medium-range Weather Forecasts. Calculations for this study were supported by the High-Performance Grid Computing Platform of Sun Yat-sen University and the China National Supercomputer Center in Guangzhou.

Open Access This article is distributed under the terms of the Creative Commons Attribution 4.0 International License (<http://creativecommons.org/licenses/by/4.0/>), which permits unrestricted use, distribution, and reproduction in any medium, provided you give appropriate credit to the original author(s) and the source, provide a link to the Creative Commons license, and indicate if changes were made.

References

- Bony S et al (2006) How well do we understand and evaluate climate change feedback processes? *J Clim* 19:3445–3482

- Cai M (2005) Dynamical amplification of polar warming. *Geophys Res Lett* 32:L22710
- Cai M, Lu JH (2009) A new framework for isolating individual feedback processes in coupled general circulation climate models. Part II: method demonstrations and comparisons. *Clim Dyn* 32:887–900
- Chang CP (2004) East Asian monsoon. World Scientific Publishing Co Ptc Ltd, Singapore, 560
- Christy JR, Norris WB, Spencer RW, Hnilo JJ (2007) Tropospheric temperature change since 1979 from tropical radiosonde and satellite measurements. *J Geophys Res* 112:D06102
- Christy JR et al (2010) What do observational datasets say about modeled tropospheric temperature trends since 1979? *Remote Sens* 2:2148–2169
- Collins M et al (2013) Chap. 12—Long-term climate change: projections, commitments and irreversibility. In: IPCC (eds) *Climate change 2013: the physical science basis*. IPCC working group I contribution to AR5, Cambridge University Press, Cambridge
- Colman RA (2001) On the vertical extent of atmospheric feedbacks. *Clim Dyn* 17:391–405
- Dee DP et al (2011) The ERA-Interim reanalysis: configuration and performance of the data assimilation system. *Q J Roy Meteorol Soc* 137:553–597
- Deng Y, Park TW, Cai M (2012) Process-based decomposition of the global surface temperature response to El Niño in boreal winter. *J Atmos Sci* 69:1706–1712
- Deng Y, Park TW, Cai M (2013) Radiative and dynamical forcing of the surface and atmospheric temperature anomalies associated with the Northern Annular mode. *J Clim* 26:5124–5138
- Ding Q, Wang B, Wallace JM, Branstator G (2011) Tropical–extratropical teleconnections in boreal summer: observed interannual variability. *J Clim* 24:1878–1896. <https://doi.org/10.1175/2011JCLI3621.1>
- Fu Q, Johanson CM (2005) Satellite-derived vertical dependence of tropical tropospheric temperature trends. *Geophys Res Lett* 32:L10703. <https://doi.org/10.1029/2004GL022266>
- Fu Q, Liou KN (1992) On the correlated K-distribution method for radiative transfer in nonhomogeneous atmosphere. *J Atmos Sci* 49:2139–2156
- Fu Q, Liou KN (1993) Parameterization of the radiative properties of cirrus clouds. *J Atmos Sci* 50:2008–2025
- Fu Q, Manabe S, Johanson CM (2011) On the warming in the tropical upper troposphere: models versus observations. *Geophys Res Lett* 38:L15704
- Gill AE (1980) Some simple solutions for heat-induced tropical circulation. *Q J R Meteorol Soc* 106:447–462
- Graversen RG, Mauritsen T, Tjernstrom M, Kallen E, Svensson G (2008) Vertical structure of recent Arctic warming. *Nature* 451:53–56
- Guan XD et al (2015) The role of dynamically induced variability in the recent warming trend slowdown over the Northern Hemisphere. *Sci Rep* 5:12669
- Hansen J et al (2002) Climate forcings in Goddard Institute for Space Studies SI2000 simulations. *J Geophys Res* 107(D18):4347. <https://doi.org/10.1029/2001JD001143>
- Hartmann DL, Larson K (2002) An important constraint on tropical cloud-climate feedback. *Geophys Res Lett* 29(20):1951. <https://doi.org/10.1029/2002GL015835>
- He Z, Wu R (2014) Indo-Pacific remote forcing in summer rainfall variability over the South China Sea. *Clim Dyn* 42(9):2323–2337
- Hu X, Li Y, Yang S, Deng Y, Cai M (2017) Process-based decomposition of the decadal climate difference between 2002–13 and 1984–95. *J Clim* 30:4373–4393
- Intergovernmental Panel on Climate Change (IPCC) (2013) *Climate change 2013: the physical science basis*. In: IPCC (eds) *Contribution of working group I to AR5*, Cambridge University Press, Cambridge
- Intergovernmental Panel on Climate Change (IPCC) (2001) *Climate change 2001: the scientific basis: contribution of working group I to the third assessment report of the intergovernmental panel on climate change*. In: Houghton JT et al (eds) *Contribution of working group I to TAR*. Cambridge Univ. Press, New York, p 881
- Intergovernmental Panel on Climate Change (IPCC) (2007) *Climate change 2007: the physical science basis*. In: S Solomon et al. (eds) *Contribution of working group I to the fourth assessment report of the intergovernmental panel on climate change*. Cambridge University Press, Cambridge, p 996
- Kosaka Y, Nakamura H (2010) Mechanisms of meridional teleconnection observed between a summer monsoon system and a subtropical anticyclone. Part I: the Pacific–Japan pattern. *J Clim* 23:5085–5108
- Lau KM, Li X, Wu HT (2002) Evolution of the large scale circulation, cloud structure and regional water cycle associated with the South China Sea monsoon during May–June, 1998. *J Meteorol Soc Japan* 80:1129–1147
- Li Y, Yang S (2016) Feedback attributions to the dominant modes of East Asian winter monsoon variations. *J Clim* 30:905–930
- Li Y, Yang S, Deng Y, Hu X, Cai M (2017) A process-level attribution of the annual cycle of surface temperature over the maritime continent. *Clim Dyn*. <https://doi.org/10.1007/s00382-017-4043-9>
- Lu JH, Cai M (2009) A new framework for isolating individual feedback process in coupled general circulation climate models. Part I: formulation. *Clim Dyn* 32:873–885
- Park TW, Deng Y, Cai M (2012) Feedback attribution of the El Niño–Southern Oscillation–related atmospheric and surface temperature anomalies. *J Geophys Res* 117:D23101
- Ramage CS (1968) Role of a tropical “maritime continent” in the atmospheric circulation. *Mon Weather Rev* 96:365–370
- Santer BD et al (2008) Consistency of modeled and observed temperature trends in the tropical troposphere. *Int J Climatol* 28:1703–1722
- Soden BJ, Held IM (2006) An assessment of climate feedbacks in coupled ocean-atmosphere models. *J Clim* 19:3354–3360
- Song X, Zhang GJ, Cai M (2014) Quantifying contributions of climate feedbacks to tropospheric warming in the NCAR CCSM3.0. *Clim Dyn* 42:901–917
- Thorne PW et al (2007) Tropical vertical temperature trends: a real discrepancy? *Geophys Res Lett* 34:L16702
- Wu R, Huang G, Du Z, Hu K (2014) Cross-season relation of the South China Sea precipitation variability between winter and summer. *Clim Dyn* 43(1–2):193–207
- Yang Y, Ren R (2017) On the contrasting decadal changes of diurnal surface temperature range between the Tibetan Plateau and southeastern China during the 1980s–2000s. *Adv Atmos Sci* 34:181–198
- Yang S, Webster PJ (1990) The effect of summer tropical heating on the location and intensity of the extratropical westerly jet streams. *J Geophys Res* 95:18705–18721
- Yang S, Lau KM, Kim KM (2002) Variations of the East Asian jet stream and Asian-Pacific–American winter climate anomalies. *J Clim* 15:306–325

Publisher's Note Springer Nature remains neutral with regard to jurisdictional claims in published maps and institutional affiliations.